Neutron-induced fission cross sections simulated from (t,pf) results

W. Younes* and H. C. Britt
Lawrence Livermore National Laboratory, Livermore, California 94551
(Received 3 October 2002; published 28 February 2003)

Neutron-induced fission cross sections on ^{235}U and ^{235}U^m targets in the incident neutron energy range $E_n = 0.1-2.5$ MeV have been deduced from surrogate ^{234}U(t,pf) measurements. The surrogate (t,pf) reaction is used to populate the same compound system as the (n,f) reaction before fission, and modeling is used to compensate for the difference in population mechanisms. The calculations presented in this paper improve on previous results by incorporating realistic angular momentum and parity distributions for the (t,p) channel, and by updating transmission-coefficient values used in the neutron-capture and emission contributions that compete with the fission process. The results are generally reliable within the 10% systematic uncertainties of the (t,pf) data.

DOI: 10.1103/PhysRevC.67.024610 PACS number(s): 25.40.−h, 25.85.Ec, 25.85.Ge

I. INTRODUCTION

Direct-reaction-fission correlation measurements allow access to many compound systems that are unavailable for neutron-induced reactions because of the lack of target material with suitable lifetimes. Previously, very simplistic models were used with fission-probability data measured [1–6] in (t,pf), $(^3\mathrm{He},df)$, $(^3\mathrm{He},tf)$ and other reactions, and with estimated neutron-induced compound-nucleus cross sections to obtain indirect estimates for (n,f) cross sections [7,8]. In this earlier work, measured fission probabilities were simply multiplied by estimated neutron compound cross sections to yield an estimated (n,f) cross section. Comparisons to cases where (n,f) cross sections had been measured directly indicated that this technique could yield estimated (n,f) cross sections with accuracy of order 10–20 % for incident neutron energies above about 1 MeV. However, below 1 MeV, there were serious discrepancies that were attributed to two possible factors. First, the conversion of fission probabilities to cross sections did not account for effects due to the difference in angular-momentum distributions in the direct and neutron-capture reactions. Second, there was considerable uncertainty in the low-energy neutron transmission coefficients available at that time. This led to an uncertainty in the calculated neutron compound-nucleus cross section. This ambiguity was illustrated in the case of the ^{3}He-induced reactions where it was shown that a constant neutron compound cross section of 3.1 barn reproduced the existing (n,f) measurements where an overlap between the data sets existed, but optical model calculations predicted an unexpected increase in compound cross section with decreasing energy below 1 MeV [8].

In more recent times there have been efforts to extend ''surrogate-reaction'' techniques to other types of neutron-induced cross sections. A new direction in this area was the recent estimate of ^{239}Pu$(n,2n)$ cross sections from the observation of γ rays in the final product ^{238}Pu [9]. Additionally, with the advent of secondary beams of radioactive species at several laboratories and the prospect of a major new facility (the Rare Isotope Accelerator), there is interest in developing techniques for simulating neutron cross sections using data from (d,p) reactions done in inverse kinematics [10]. Many of the statistical-model and nuclear-structure considerations discussed in this paper in relation to the inference of (n,f) cross sections from direct-reaction fission data are also present in the interpretation of data for these proposed surrogate reactions.

In the present paper we present an analysis of fission-probability data from the ^{234}U(t,pf) reaction to yield estimated neutron cross sections for ^{235}U that can be compared to the evaluated nuclear data file (ENDF) results [11]. The ENDF evaluation is based on a covariance analysis of experimental data and carries uncertainties of less than 2% for the ^{235}U(n,f) cross section below $E_n = 3$ MeV. We attempt to improve on the previous surrogate methods for estimating (n,f) cross sections by decomposing the measured fission probabilities into its components as a function of spin/parity using a statistical model developed to fit the fission-probability data and extract fission-barrier parameters [3]. Then these probabilities can be combined with improved estimates of neutron transmission coefficients and summed to give a more realistic (n,f) estimate. In addition to fission of the ^{235}U $J^\pi = 7/2^-$ ground state, the detailed model can be used to estimate fission cross sections of the $1/2^+$ isomer state at 77 eV. Inputs to the statistical model have been evaluated and updated where appropriate, and the sensitivity of the (n,f) estimates to various inputs has been evaluated. In order to minimize effects due to the uncertainties in the discrete levels and continuous level densities used in the calculations, a technique is developed to renormalize the results using the experimental fission-probability measurements. Improvements necessary for the development of a more predictive approach to estimating (n,f) cross sections are discussed.

II. MODEL

A. Fission probabilities

The double-humped fission model used to calculate fission probabilities is taken from earlier papers [1–6] where it has been used to extract fission-barrier parameters for a large

*Electronic address: younes@llnl.gov

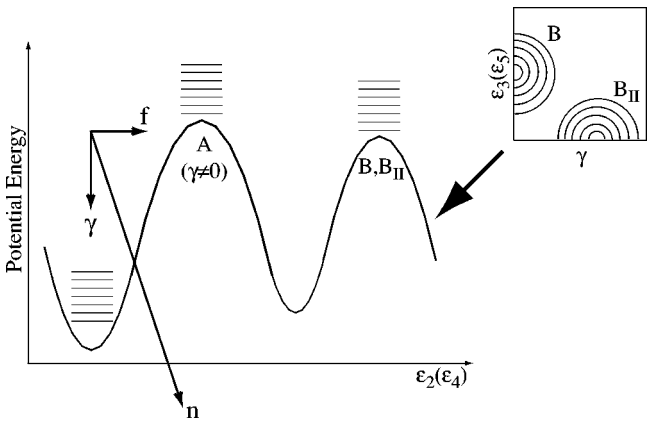

FIG. 1. Schematic representation of the statistical fission model used. The inset shows the difference between barriers B and B_{II} encountered along parallel fission paths: barrier B has a static octupole deformation, whereas barrier B_{II} is triaxial.

number of actinide nuclei from measured fission-probability data. In the present work, the version of this model that assumes complete damping of the flux as it proceeds to fission across the two peaks of the fission barrier is used. This approach neglects the resonant penetration of the two-peaked barrier which is important near threshold, but the complete damping limit is most appropriate for the above-barrier energy region of interest. A truly comprehensive model which would allow for resonant penetration, different symmetries at the three saddles and parallel paths at the second barrier has never been attempted and is beyond the scope of this work.

Schematically this complete damping model is illustrated in Fig. 1. In the present version of the model, fission proceeds through an inner barrier A and then through one of two parallel paths through barrier B or B_{II}. Evidence for the existence of a parallel path to fission through barrier B_{II} can be found in the paper by Gavron *et al.* [12], which reproduces fission-probability data from both $^{236}\mathrm{U}(t,pf)$ and $^{238}\mathrm{U}(\gamma,f)$ reactions in a consistent manner.

The fission probability is simply given by the ratio of the effective number of open fission channels divided by the sum of the effective number of open channels available for fission, neutron and gamma de-excitation. The effective number of open channels for a decay process i from a compound state with excitation energy E_x and spin/parity J^π is defined in terms of its decay width $\Gamma_i(E_x,J^\pi)$ and the density of levels $\rho(E_x,J^\pi)$ by

$$N_i(E_x,J^\pi) \equiv 2\pi\rho(E_x,J^\pi)\times\Gamma_i(E_x,J^\pi). \tag{1}$$

The effective number of fission states, N_f, is obtained from the number of states available at the γ-asymmetric saddle A and the sum of the states available at the mass-asymmetric and γ-asymmetric second saddles along parallel paths to fission, B and B_{II}. The effective number of open channels for neutron, N_n, and γ ray, N_γ, emission are calculated using standard Hauser-Feshbach formalisms.

The (t,pf) reaction is thought to proceed in two sequential steps: first a compound system is formed by a direct (t,p) reaction and then, after a comparatively long time, the equilibrated nucleus fissions. The (t,pf) fission probabilities as a function of excitation energy E_x are calculated by summing the contributions from individual J^π compound states. The individual J^π components are obtained from the direct-reaction (t,p) population probabilities $P_{(t,p)}$ and the fission probability P_f from a given state (E_x,J^π) using

$$P_{(t,pf)}(E_x) = \sum_{J^\pi} P_{(t,p)}(J^\pi) P_f(E_x,J^\pi), \tag{2}$$

where the direct-reaction population probabilities are determined by distorted-wave Born approximation (DWBA) calculations which are further described in Sec. II C. In this case the energy dependence for $P_{(t,p)}$ has been suppressed since $P_{(t,p)}$ does not change significantly with energy over the excitation energy region of interest here.

Similarly the neutron-induced fission probability can be obtained by summing over the same $P_f(E_x,J^\pi)$ values weighted by calculated neutron compound formation probabilities,

$$P_{(n,f)}(E_x) = \sum_{J^\pi} P_{CN}(E_x,J^\pi) P_f(E_x,J^\pi), \tag{3}$$

where the compound-nucleus formation probabilities, P_{CN}, are given in terms of the compound-nucleus formation cross sections σ_{CN} (see Sec. II C):

$$P_{CN}(E_n,J^\pi) \equiv \frac{\sigma_{CN}(E_n,J^\pi)}{\sum_{J^\pi} \sigma_{CN}(E_n,J^\pi)}. \tag{4}$$

Here the excitation-energy dependence has been converted to neutron energy using the relation $E_n = E_x - B_n$ where B_n is the neutron binding energy. The estimated neutron-fission cross section is then obtained from

$$\sigma_{(n,f)}(E_n) = \sum_{J^\pi} \sigma_{CN}(E_n,J^\pi) P_f(E_x,J^\pi). \tag{5}$$

There are uncertainties in the discrete and continuous levels used in the N_i calculations and discontinuities in the regions where discrete and continuous level densities are joined (see further discussion below). These discontinuities tend to produce anomalous structures in the $P_{(t,pf)}(E_x)$ function which are then mirrored in the $\sigma_{(n,f)}(E_n)$ function. In order to remove this anomalous structure, the estimated (n,f) cross section is further renormalized to the measured $P_{(t,pf)}$ data as follows:

$$\sigma^{(\mathrm{ren})}_{(n,f)}(E_n) \equiv \sigma_{(n,f)}(E_n) \times \frac{P^{(\mathrm{expt})}_{(t,pf)}(E_x)}{P^{(\mathrm{calc})}_{(t,pf)}(E_x)}$$
$$= P^{(\mathrm{expt})}_{(t,pf)}(E_x) \times \sigma_{CN}(E_n) \times \left[\frac{\sum_{J^\pi} P_{CN}(E_n, J^\pi) P_f(E_x, J^\pi)}{\sum_{J^\pi} P_{(t,p)}(J^\pi) P_f(E_x, J^\pi)} \right], \quad (6)$$

where $\sigma_{CN}(E_n) \equiv \Sigma_{J^\pi} \sigma_{CN}(E_n, J^\pi)$, to produce a more robust estimate of the cross section. The term in square brackets in Eq. (6) contains all the dependence on angular momentum and population mechanisms. This term, labeled $F(E_n)$, can be written in a more suggestive form

$$F(E_n) = 1 + \frac{\sum_{J^\pi} [P_{CN}(E_n, J^\pi) - P_{(t,p)}(J^\pi)] P_f(E_x, J^\pi)}{\sum_{J^\pi} P_{(t,p)}(J^\pi) P_f(E_x, J^\pi)}, \quad (7)$$

that makes manifest the behavior of the estimated (n,f) cross section when the population probabilities from the neutron-capture and (t,p) reactions are identical; in that case $F(E_n)$ becomes equal to 1 and the renormalized cross section in Eq. (6) is simply the product of the experimental $P_{(t,pf)}$ data and the calculated compound-nucleus cross section, as was done in earlier work [8]. The same simplification occurs if the $P_f(E_x, J^\pi)$ probabilities are independent of J^π. The factor $F(E_n)$ is discussed further in Sec. III and in the Appendix. In the remainder of this paper, we will drop the "(ren)" superscript for $\sigma_{(n,f)}$ and it will be implicitly assumed that the (n,f) cross section has been renormalized as in Eq. (6), unless otherwise specified.

The statistical fission model used to produce the probabilities $P_f(E_x, J^\pi)$ in Eq. (2) is discussed next, with additional details given in Secs. II B and II C. From a compound state with excitation energy E_x and spin/parity J^π three possible decay paths are considered: γ decay, neutron emission, and fission, represented by the number of effective open channels N_γ, N_n, and N_f in each case, respectively. Then

$$P_f(E_x, J^\pi) \equiv \phi(E_x, J^\pi) \frac{N_f(E_x, J^\pi)}{N_\gamma(E_x, J^\pi) + N_n(E_x, J^\pi) + N_f(E_x, J^\pi)}. \quad (8)$$

The coefficient $\phi(E_x, J^\pi)$ is a width-fluctuation correction factor for both neutron emission and fission, assuming a Porter-Thomas distribution [13] in both cases. This correction is an extension of the formula in Ref. [14] to the case where both fission and neutron fluctuations may be important. Following Moldauer [15], the expression for $\phi(E_x, J^\pi)$ can be written as the integral

$$\phi(E_x, J^\pi) = \int_0^\infty dt\, e^{-p_\gamma t} \frac{1}{\left(1 + \frac{2p_f t}{\nu_f}\right)^{\nu_f/2+1} \left(1 + \frac{2p_n t}{\nu_n}\right)^{\nu_n/2}}, \quad (9)$$

where the $p_i \equiv N_i / \Sigma_i N_i$ for the $i = \gamma, n, f$ channels are the uncorrected decay probabilities. The degrees of freedom ν_n and ν_f for the Porter-Thomas distributions are taken equal to N_n and N_f respectively or 1, whichever is larger. This prescription for the degrees of freedom was chosen to give $\phi(E_x, J^\pi)$ a smooth energy dependence, and to provide a consistent treatment of the neutron and fission channels and a rapid damping of the many-partial-wave neutron-width fluctuations. The factor $\phi(E_x, J^\pi)$ introduces at most a 30% correction to the calculated fission probabilities.

The statistical γ-ray decay is assumed to proceed via electric dipole transitions, and is given by

$$N_\gamma(E_x, J^\pi) = 2\pi C_\gamma A^{2/3} \sum_{J'=|J-1|}^{J+1} \int_0^{E_x} d\epsilon \rho_\gamma(\epsilon, J', -\pi) \times (E_x - \epsilon)^3, \quad (10)$$

where A is the mass number of the compound system, and C_γ is a normalization constant fixed at 2×10^{-8} MeV^{-3}, in accordance with Ref. [3]. The level density ρ_γ refers to states in the first well of the compound nucleus. In the case of γ decay in the first well of ^{236}U, the energy integral in Eq. (10) reduces to a sum over discrete states in ^{236}U below the pairing-gap energy, $2\Delta = 1180$ keV; however these discrete levels do not play an important role in the present calculations. The discrete levels used are shown in Fig. 2. The continuous level density functions are discussed in Sec. II B.

The neutron emission channel is described by a standard statistical formula

$$N_n(E_x, J^\pi) = \sum_i \sum_{j=|j_i - J|}^{j_i + J} \sum_{\ell=|j-1/2|}^{j+1/2} T_{\ell j}(E_x - B_n - \epsilon_i)\, \delta_{\pi_i, \pi(-1)^\ell} + \sum_{J'} \sum_{j=|J'-J|}^{J'+J} \sum_{\ell=|j-1/2|}^{j+1/2} \int_{\Delta_n}^{E_x - B_n} d\epsilon \times \rho_n(\epsilon, J', \pi(-1)^\ell) T_{\ell j}(E_x - B_n - \epsilon), \quad (11)$$

written here explicitly in terms of discrete-level and continuous level-density contributions. The summation over index i in the first term covers all discrete states (ϵ_i, j_i, π_i) below the maximum excitation energy $E_x - B_n$ or the pairing energy Δ_n, whichever is smaller. In the case of neutron emission from ^{236}U to ^{235}U, the neutron binding energy is $B_n = 6.545$ MeV, and the adopted pairing energy is $\Delta_n = 690$ keV [16]. The transmission coefficients are denoted by $T_{\ell j}$, and ρ_n is the level density in the neutron-out channel.

Fission through a barrier b is given by the standard Hill-Wheeler form

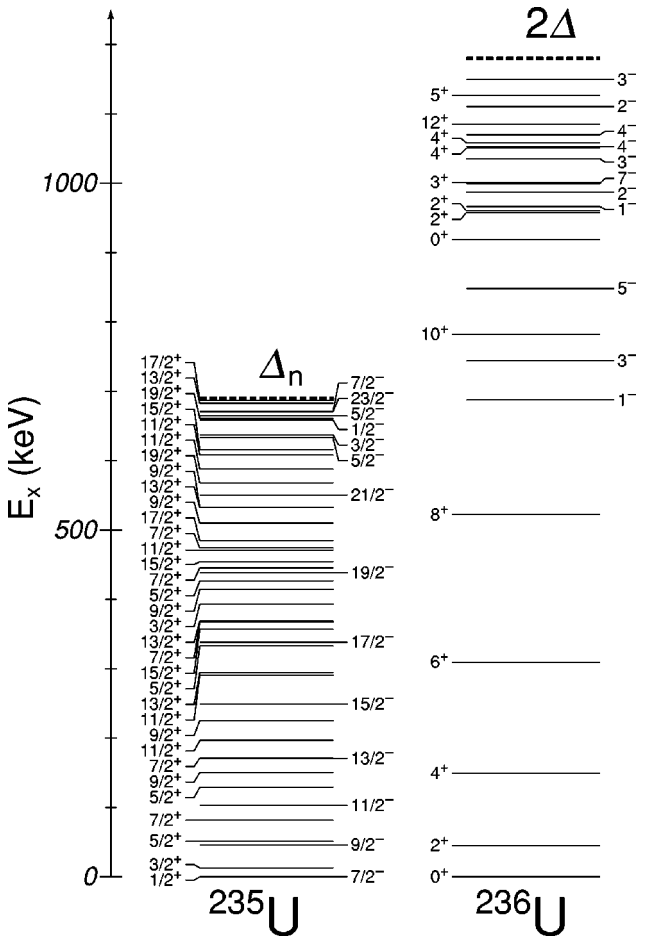

FIG. 2. First-well discrete levels used in the calculations. The spin/parity label appears on the right for positive-parity levels and on the left for negative-parity levels. The pairing gaps Δ_n for the odd-A system and 2Δ for the even-even nucleus are marked by dotted lines.

$$N_b(E_x,J^\pi)=\sum_i \frac{\delta_{J,j_i}\delta_{\pi,\pi_i}}{1+\exp\left(2\pi\dfrac{\epsilon_i+E_b-E_x}{\hbar\omega_b}\right)} + \int_{2\Delta_b}^{\infty} d\epsilon \frac{\rho_b(\epsilon,J,\pi)}{1+\exp\left(2\pi\dfrac{\epsilon+E_b-E_x}{\hbar\omega_b}\right)}, \quad (12)$$

where E_b and $\hbar\omega_b$ characterize the height and curvature of the barrier. The discrete-level and continuous level-density contributions have again been written explicitly. The summation over index i in the first term extends over discrete transition states above the barrier with excitation energy ϵ_i, and spin/parity j_i/π_i up to the maximum energy E_x-E_b, or the pairing-gap energy $2\Delta_b$, whichever is smaller.

In the fission model depicted in Fig. 1, three barriers are considered: *A*, *B*, and B_{II}. The fissioning nucleus traverses the inner barrier *A* and proceeds through one of two parallel fission paths, through barrier *B* or B_{II}. Fission through the combined barriers is given by the non-resonant penetration formula

$$N_f(E_x,J^\pi)=\frac{N_A(N_B+N_{B_{II}})}{N_A+N_B+N_{B_{II}}}. \quad (13)$$

In the present calculations, we took $\hbar\omega_A=0.90$ MeV, $\hbar\omega_B=0.65$ MeV, and $\hbar\omega_{B_{II}}=0.90$ MeV. These are typical values of the barrier curvature parameters for the actinide region [3]. Variation of these values within errors produces negligible changes in the final deduced $\sigma_{(n,f)}$ values in this paper (see the Appendix). The three barrier heights, the only adjustable parameters in the model, were optimized to reproduce the $P_{(t,pf)}$ data. The remaining inputs to the model were fixed based on physically reasonable assumptions.

B. Input level densities and discrete levels

At excitation energies near the fission barrier and near the neutron binding energies, the fission probabilities can be strongly affected by the details of the specific states available for decay by either fission or neutron emission. In the energy regions below the pairing gaps it is essential to carry out the calculations using discrete levels with specified spin, parity, and excitation energy. At excitations above the pairing gaps in even-even and odd-*A* nuclei the levels become dense enough that a continuous statistical level density can be used. In the present model discrete spectra are used for even-even systems up to the pairing gaps $(\Delta_p+\Delta_n)$ and for odd-*A* systems up to Δ_p or Δ_n. For an odd-odd system the continuous level density would be used at all energies. The discrete spectra used in the first well for ^{235,236}U are obtained from standard compilations [17,18], and shown in Fig. 2.

Figure 3 shows vibrational states appropriate for each barrier. The lowest $K^\pi=0^+,2^+,4^+$ and $0^-,1^-,2^-$ states were obtained from results of fitting direct-reaction-fission angular correlation studies [1,2] and from fits to sub-barrier resonances in (d,pf), (t,pf), and (γ,f) studies [3,4,19] (see Fig. 3). These experiments are not sensitive enough to identify more than the lowest vibrational band with each *K*, and they give only approximate locations for these bands. These vibrational states were then coupled in pairs to form the remaining levels in Fig. 3. Following Griffin [20], the energy of the two-phonon state was taken to be the sum of the energies of the individual states. Rotational bands were constructed on top of the vibrational states up to the pairing-gap energy, using a moment of inertia $\mathcal{I}$ given by $\hbar^2/2\mathcal{I}=7$, 5, and 7 keV for barriers *A*, *B*, and B_{II}, respectively.

Beyond the pairing-gap energy, the continuous level densities were taken directly from an earlier fission-probability model [19]. In that model, a continuous state density $w(E)$ is obtained from the permutation of particles in the shell-corrected single-particle spectra at the appropriate saddle and ground state configurations using a Strutinski renormalization process. These estimates incorporate appropriate pairing interactions using pairing gaps obtained directly from the same single-particle spectra. Level densities for specific J^π are then obtained using the microscopic level density enhancement factors from Bjørnholm, Bohr, and Mottelson [21]. The level densities obtained for ^{235,236}U at the appropriate deformations are shown in Fig. 4. A detailed descrip-

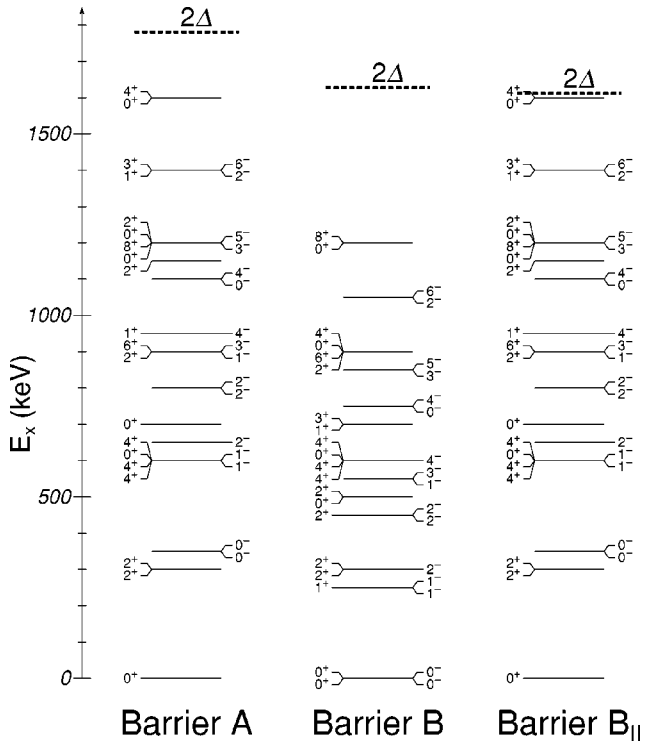

FIG. 3. Vibrational transition states used in the calculations, given for each barrier and labeled by their K^{π} quantum numbers. The actual levels are generated by building rotational band members on top of each vibrational state with moment of inertia $\mathcal{I}$ given by $\hbar^2/2\mathcal{I}=7$, 5, and 7 keV for barriers *A*, *B*, and B_{II}, respectively. Note that, in the case of the $K^{\pi}=0^-$ bands, the first level has spin/parity 1^-. The dashed line denotes the pairing-gap energies.

tion of the level-density calculations is given in Ref. [6]. The level densities used in the present work were calculated without adjustable parameters and the discrete levels were also generated in a systematic way up to the pairing gap. This approach was preferred because it does not introduce additional degrees of freedom into the fission-model calculation and the fit to the $P_{(t,pf)}$ data. The price that is paid for this choice is the mismatch observed between discrete and continuum regions in Fig. 4. Sensitivity tests in the Appendix show that, because of the renormalization in Eq. (6), improving the matching between these regions does not significantly affect the deduced (n,f) cross section (see, e.g., tests 1 and 7).

In general terms, the continuous level densities used in this paper can be written in the form

$$\rho(E_x,J,\pi)=f_{\pi}k(U)f(J;\sigma_{\perp}^2)w(U), \tag{14}$$

where $\mathrm{U}\equiv E_x-\Delta_p-\Delta_n$ is the excitation energy corrected for pairing, f_{π} gives the dependence on parity π (in practice $f_-=f_+=1/2$), and the spin dependence is given by the function

$$f(J;\sigma^2)\equiv\frac{2J+1}{2\sigma_{\perp}^2}\exp\left(-\frac{J(J+1)}{2\sigma_{\perp}^2}\right), \tag{15}$$

with $\sigma_{\perp}=5.45$. The collective enhancement factors are broken down in terms of the symmetry at the deformation of interest,

$$k(U)=\begin{cases}\sigma_{\perp}^2/[\sqrt{2\pi}\times\sigma_{\parallel}(U)] & \text{axially symmetric}\\ 2\sigma_{\perp}^2/[\sqrt{2\pi}\times\sigma_{\parallel}(U)] & \text{reflection asymmetric}\\ 2\sigma_{\perp}^2 & \text{triaxial,}\end{cases} \tag{16}$$

where $\sigma_{\parallel}(U)$ is calculated along with $w(U)$ by the combinatorial method described above.

C. Transmission coefficients and formation cross sections

The evaluation of Eqs. (2) and (5) requires an estimate of the population cross sections in the (t,p) and neutron-induced reactions as a function of J, π, and E_x. Figure 5 shows a comparison of calculated populations via the (t,p), (d,p) and neutron-induced (at $E_n=0.5$ and 2.0 MeV) reactions. The (t,p) and (d,p) results are taken from Ref. [3]. The transfer cross sections $\sigma(\ell)$ are taken directly from a DWUCK calculation [22] and multiplied by a requisite $(2\ell+1)$ normalization factor. As a check, calculations done using the code DWUCK4 [22] show that for proton detection angles greater than 90°, varying optical parameters, the beam energy and excitation energy within reasonable extremes does not affect the neutron fission cross section estimates in this paper. For neutron capture, the population cross sections are discussed in more detail below.

It can be seen in Fig. 5 that the decomposition of the fission probability into spin/parity components is a necessary step in the $\sigma_{(n,f)}$ calculation, since the formation cross sections from the (t,p) and neutron-induced (n) reactions are quite different, especially for $E_n=0.5$ MeV. For $E_n=2.0$ MeV, the (t,p) and (n) distributions are more alike, although the neutron-induced reaction is more akin to the (d,p) process for comparable energy transfers, as might be expected. The calculation of the formation process is described in this section.

The population probability in the (t,p) reaction, needed in Eq. (2), is obtained using the simple formalism described by Back *et al.* [3], wherein the expression

$$S_{(t,p)}(J^{\pi})=\frac{1}{2}(2J+1)\exp\left(-\frac{\left(J+\frac{1}{2}\right)^2}{2\sigma_{\perp}^2}\right)\times\frac{\sum_{J'=|J-I_0|}^{J+I_0}\sigma_{\ell J'\pi}}{(J+I_0)-|J-I_0|+1}, \tag{17}$$

where I_0 is the target spin, is normalized with respect to all possible spin/parities formed in the compound nucleus to give the formation probability

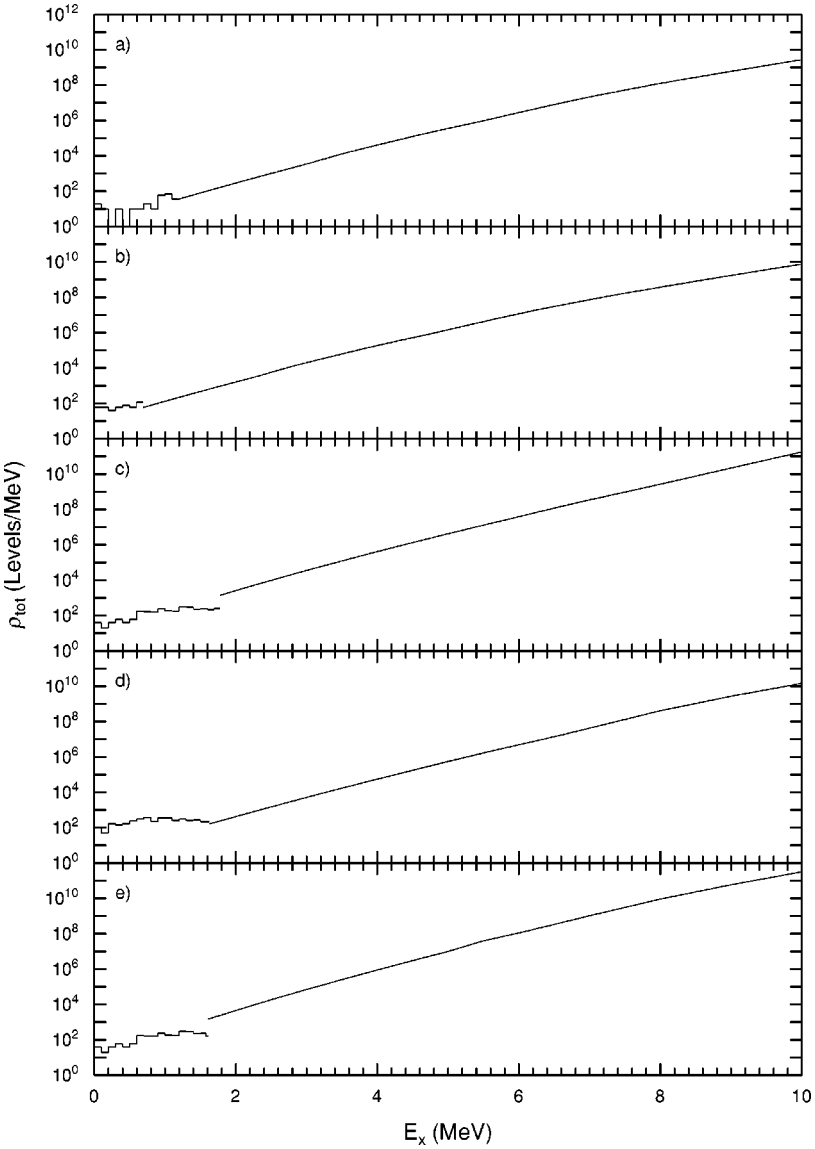

FIG. 4. Total level densities $[\rho_{\rm tot}(E_x) \equiv \Sigma_{J^\pi}\rho(E_x,J^\pi)]$ appropriate for (a) the first well in ^{236}U, (b) the first well in ^{235}U, (c) barrier *A*, (d) barrier *B*, and (e) barrier B_{II}.

$$P_{(t,p)}(J^\pi)=\frac{S_{(t,p)}(J^\pi)}{\sum_{J^\pi} S(t,p)(J^\pi)}. \tag{18}$$

It is assumed that the two neutrons transferred in the (t,p) reaction are in an $\ell=0$ relative state and, therefore, in Eq. (17),

$$\sigma_{\ell J'\pi}=\delta_{\ell,J'}\delta_{\pi,(-1)^\ell}\times\sigma_\ell\,. \tag{19}$$

The dimensionless formation cross section for (t,p) reactions, σ_ℓ, is taken from Ref. [3], and displayed in Fig. 5.

The neutron-induced cross-section and the neutron-decay calculations require neutron transmission coefficients for relevant transferred orbital and total angular momenta (ℓ,j) as a function of energy. These inputs have been obtained using optical models with accepted parameter sets and a coupled-channel formalism to calculate transmission coefficients [23]. Neutron capture into compound states with specific quantum numbers (E_x,J^π) is given by [24]

$$\sigma_{CN}(E_n,J^\pi)=\pi\lambda\!\!\!^{-2}\frac{(2J+1)}{(2\times\frac{1}{2}+1)(2I_t+1)} \times\sum_{S=|I_t-1/2|}^{I_t+\frac{1}{2}}\sum_{\ell=|J-S|}^{J+S}T_\ell(E_n)f_\ell(\pi), \tag{20}$$

where the transmission coefficients $T_{\ell j}$ are averaged over the possible alignments of the intrinsic spin:

$$T_\ell(E_n)\equiv\frac{1}{2\ell+1}[(\ell+1)T_{\ell,\ell+1/2}(E_n)+\ell T_{\ell,\ell-1/2}(E_n)]. \tag{21}$$

The weighting factor $f_\ell(\pi)$ in Eq. (20) ensures parity conservation in the reaction:

$$f_\ell(\pi)=\frac{1}{2}|\pi+(-1)^\ell\pi_t\pi_n|. \tag{22}$$

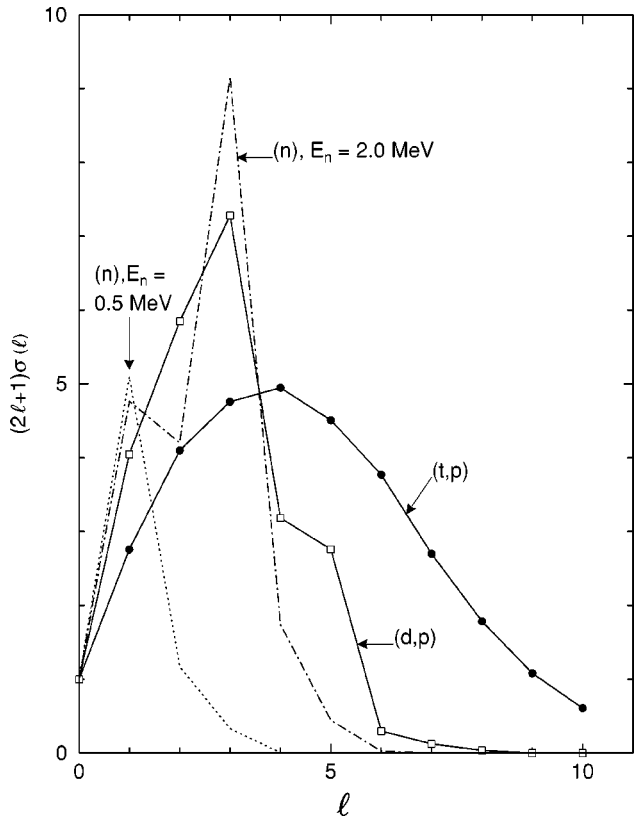

FIG. 5. Relative cross sections for the (t,p), (d,p), and neutron-induced (n) reactions at $E_n = 0.5$ and 2.0 MeV, as a function of transferred orbital angular momentum ℓ. Lines are drawn connecting the (t,p), (d,p), and (n) points to guide the eye.

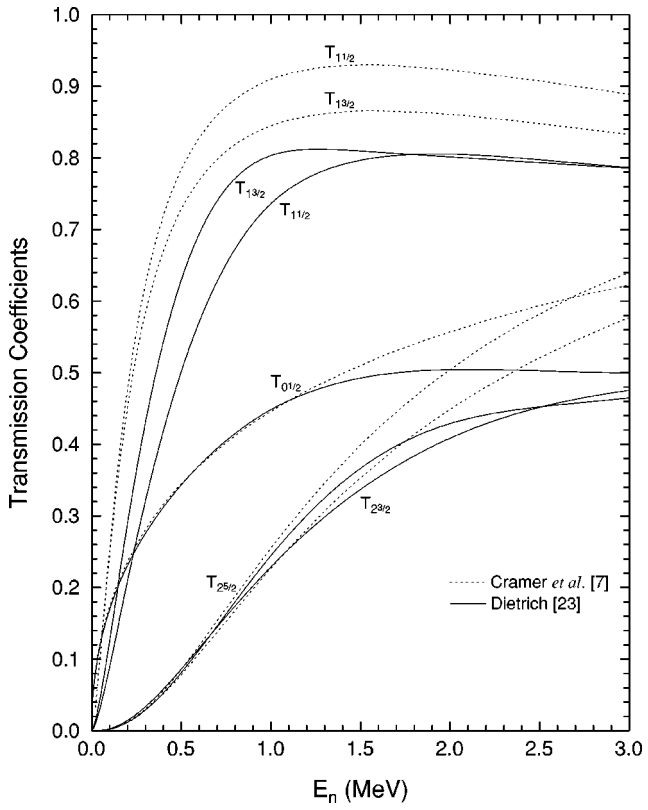

FIG. 6. Neutron transmission coefficients $T_{\ell j}$ calculated by Dietrich [23] and used in the present work, compared to older calculations using the ABACUS program (Cramer *et al.* [7]). only the coefficients with $\ell \leqslant 2$ are shown.

A sample of the more important transmission coefficients used is compared in Fig. 6 to older calculations using the ABACUS code [7]. It is seen that the trend in the new Dietrich calculations [23] while showing some structure are generally much closer to the empirical constant value successfully used in previous work [8] (see Fig. 7).

III. RESULTS

A. Fit to ^{234}U(t,pf) data

There are two available sets of (t,pf) data that were published by Britt *et al.* in 1968 [1] and Back *et al.* in 1974 [3]. The data sets differ significantly in the region just below the neutron binding energy as shown in Fig. 8. The experimental techniques and objectives in the two experiments were quite different. The 1968 experiment involved a detailed measurement of the fission-fragment angular correlations with the goal of identifying the positions of major collective bands at the fission saddle point. It used a small solid-angle telescope for proton identification and measurement. The triton bombarding energy of 18 MeV with proton detection at 140° shifts most of the carbon and oxygen contaminant peaks out of the proton energy region of interest in this work. The 1974 experiment was aimed at measuring sub-barrier resonance structures with relatively low fission probabilities. It used a bombarding energy of 15 MeV, a large solid angle proton telescope at 90° and a single large-angle annular fission detector at 180° in order to get maximum coincidence statistics. This configuration resulted in strong C and O contaminant peaks near and just above B_n and limited the energy range that could be studied to about 0.5 MeV above B_n.

In these experiments the major problem in determining a fission probability is extracting the singles cross section for ^{235}U(t,p) due to the large background of protons from reactions on carbon and oxygen included in the targets. The excitation energy regions where the ^{235}U(t,p) is obscured by C and O contaminants is shown by open symbols in Fig. 8 for both experiments. In general the ^{235}U(t,p) singles were determined by extrapolating underneath the observed C and O peaks. In the 1968 experiments this was much easier because of the smaller kinematic spreads and because a separate set of measurements was also performed using an even smaller solid angle for the particle telescope. Additionally, in the 1968 experiment the fission fragment angular correlations were measured directly, which made the integration of the distribution over 4π more reliable. For this reason the $P_{(t,pf)}$ data for the region of the neutron binding energy and higher is believed to be more reliable in the 1968 experiment.

In the present work we refit the 1968 data. The barrier heights E_A and E_B were adjusted to reproduce the $P_{(t,pf)}$ data below the neutron binding energy, and the barrier height $E_{B_{II}}$ was taken to be the same as in ^{238}U, as established in Ref. [12] (see the Appendix for the effect of different fitting

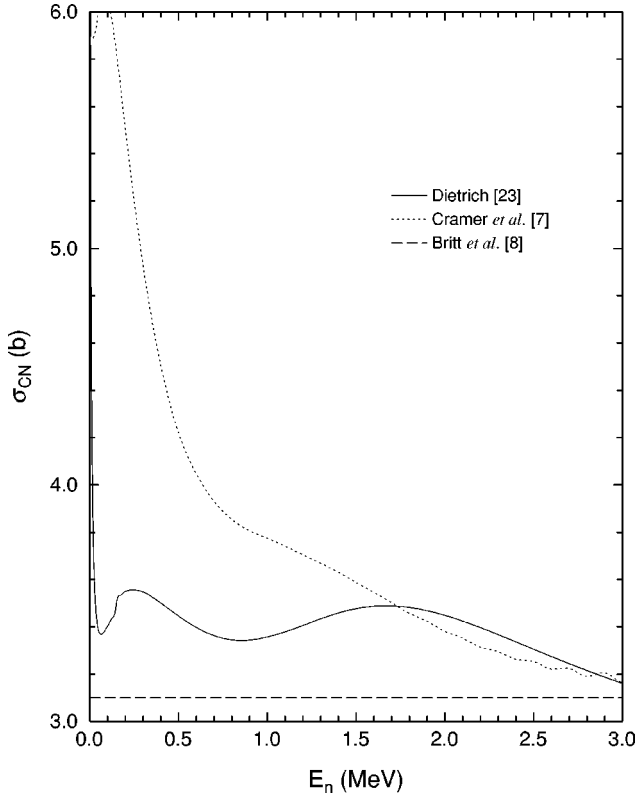

FIG. 7. Compound-nucleus cross section for the neutron-capture reaction calculated using transmission coefficients from Dietrich [23] and from older ABACUS results (Cramer *et al.* [7]), compared to the constant cross section used by Britt *et al.* [8].

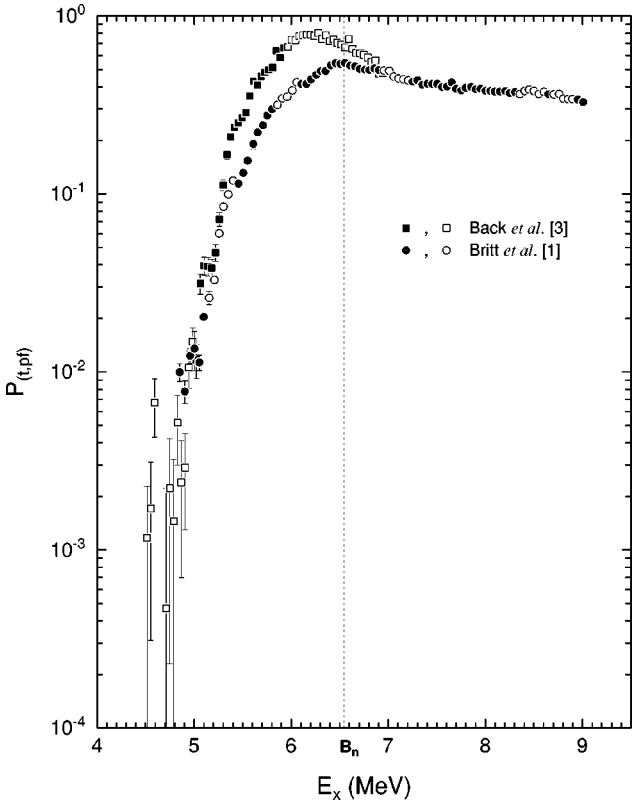

FIG. 8. Comparison of $P_{(t,pf)}$ data from Britt *et al.* [1] and Back *et al.* [3] experiments. Open symbols represent regions where the data were contaminated by carbon and oxygen peaks. Uncontaminated data are represented by filled symbols. The dotted line marks the neutron binding energy.

prescriptions). Barrier heights of $E_A=6.2$ MeV, $E_B=6.0$ MeV, and $E_{B_{II}}=6.4$ MeV were used in the fit. The A and B barrier heights are somewhat higher than those obtained by Back *et al.* [3] because of the differences in the data and in the level-density formulations used. The results are shown in Fig. 9. The fit is reasonable in the barrier region but overshoots the data in the region near B_n and undershoots in the region near $E_x=8$ MeV. The origin of these deviations is not clear. In the region of $E_x \approx B_n$ there is a significant difference between the two data sets so the problem could be experimental. In the region near 8 MeV the dip may be due to problems in the level densities in the regions where the discrete levels transition to a continuous level density. It is the presence of this anomalous structure that led to the necessity for the renormalization procedure discussed in Sec. II A.

The $P_{(t,pf)}$ calculations involve summing the individual $P_f(J^\pi)$ over all J^π weighted by the partial cross sections shown in Fig. 5. Thus, it is possible to examine the individual P_f distributions to obtain insight into the factors influencing $P_{(t,pf)}$ in the region near threshold. Figure 10 shows the P_f distributions for individual J states with (a) positive and (b) negative parities. It is seen that the behavior in the threshold region is driven by two components. First fission proceeds through the $K=0^+$ and 0^- bands with natural parity states (0^+, 2^+, 4^+, ...) and (1^-, 3^-, 5^-, ...). Then at higher excitation energies the vibrational $K=2^+$ and 1^- bands become available and bring in the rest of the states except for the 1^+ and 0^- since in this model it is difficult to make 1^+ or 0^- states at excitations below the pairing gap. The first 1^+ arises from a two-phonon excitation of the $K=0^-$ and 1^- according to the model of Griffin [20]. Therefore, in this model, fission through these states is inhibited in the low-energy (n,f) region. This effect sets the stage for possible deviations that are tied to target spin in low-energy fission cross sections. For example, in ^{235}U with ground state $J^\pi=7/2^-$ there is little involvement of 1^+, 0^- fissioning states at low energies. For ^{239}Pu, with ground state $J^\pi=1/2^+$, it can be expected that 1^+, 0^- states will be strongly excited in the region below $E_n=1$ MeV and that their fission may be inhibited. In ^{235}U there is also a low lying isomer (at 77 eV) with $J^\pi=1/2^+$ which in principle could allow an experimental investigation of this effect.

The $P_f(E_x,J^\pi)$ results shown in Fig. 10 also illustrate that for $E_n>1.5$ MeV ($E_x>8.0$ MeV) the fission probabilities converge and no longer show a significant dependence on J^π. This is because this region is now dominated by the statistical level densities which have similar spin distributions that cancel out in the ratio of the number of open channels, N_f/N_n. This result verifies the validity of the earlier observation [7,8] that direct-reaction fission probabilities could be transformed to (n,f) cross sections simply by multiplying by the neutron compound-nucleus cross section.

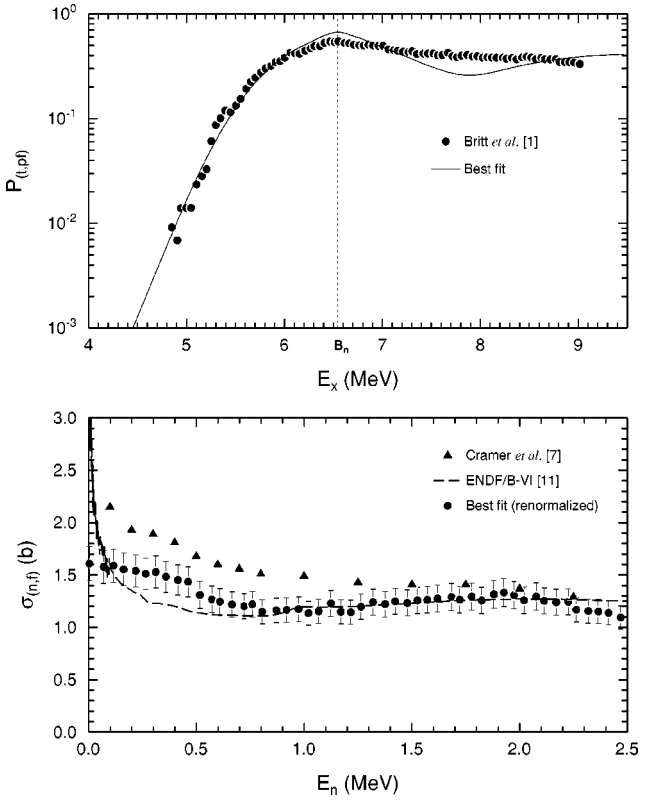

FIG. 9. Best fit to the $P_{(t,pf)}$ data (top panel), and estimated (n,f) cross section compared to the original result of Cramer *et al.* [7] and the evaluated ENDF/B-VI values (bottom panel). The dotted line in the top panel indicates the neutron-binding energy value. The error bars on the estimated $\sigma_{(n,f)}$ values correspond to a 10% systematic uncertainty in the $P_{(t,pf)}$ data. The Cramer *et al.* cross section carries the same 10% uncertainty associated with the $P_{(t,pf)}$ data (error bars not shown).

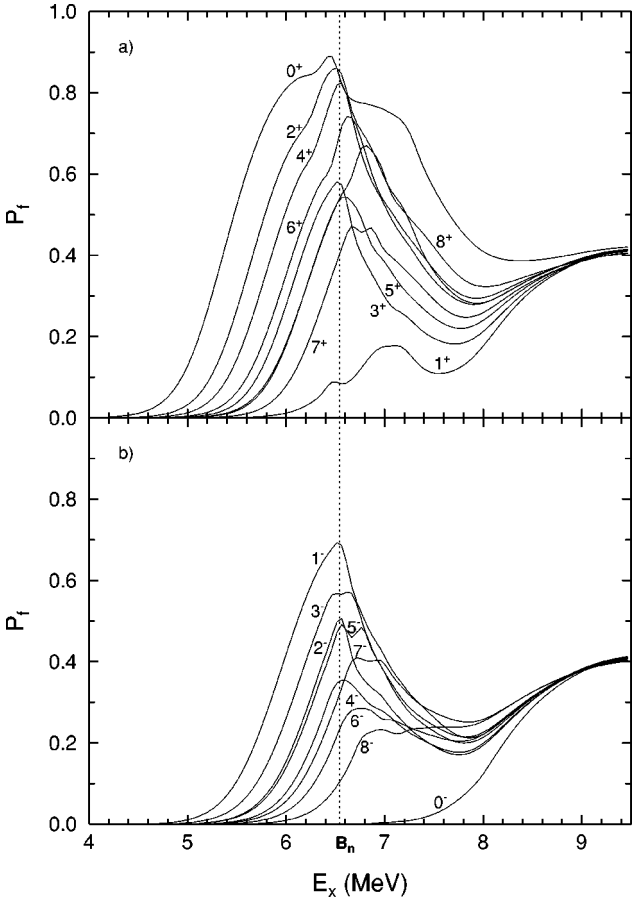

FIG. 10. Best-fit values of the individual fission probabilities $P_f(E_x,J^\pi)$, as a function of excitation energy E_x of the compound nucleus. The positive-parity probabilities are plotted in panel (a), while the negative-parity ones are shown in panel (b). The dotted vertical line indicates the neutron-binding energy value.

B. Simulated (n,f) cross section

Figure 9 shows the estimated (n,f) cross section results from the model with P_f renormalized to the (t,pf) data. The result is compared to the evaluated ENDF/B-VI data for ^{235}U [11]. It is seen that the simulated cross sections generally agree with ENDF/B-VI within the estimated systematic errors ($\pm 10\%$) published for the (t,pf) data except for an approximate 20% overshoot in the region of 0.2–0.5 MeV. This is an energy region where both the data and the calculated neutron compound cross sections could have increased uncertainties and the interpretation of this discrepancy is unclear. However, overall the agreement between the simulated cross section and ENDF/B-VI is remarkably good. This comparison involves no adjustable ''parameters'' so that the agreement implies that this procedure, the absolute fission probability measurements, and the calculated neutron compound cross sections are collectively accurate to approximately 10%. (Although the possibility of larger errors which cancel in the product cannot be ruled out.) The ^{235}U(n,f) cross section deduced in this work is also compared to the original estimate by Cramer *et al.* [7] in Fig. 9. Cramer *et al.'s* results are based on the same $P_{(t,pf)}$ data as the present work, but rely on older transmission-coefficient calculations and do not incorporate spin and parity in the calculation. Cramer *et al.'s* cross section values, plotted in Fig. 9, are averaged over 100-keV intervals below $E_n=1$ MeV, and over 250-keV intervals above $E_n=1$ MeV, as was done in Ref. [7]. The (n,f) cross section estimated in the present work is clearly in much better agreement with the ENDF/B-VI evaluation than the original result, especially for incident neutron energies below 1 MeV.

Because of the renormalization technique used in Eq. (6) it is not possible to extrapolate the inferred cross sections outside the energy range covered in the (t,pf) measurement ($E_n=0.1-2.5$ MeV). Possible improvements that could give more predictive powers to this technique will be discussed in the Appendix. A following paper will show calculated surrogate fission cross sections obtained from (t,pf) data for a series of other Th, U, and Pu isotopes, many of which are not directly measurable.

As discussed above, there is a predicted dependence of the (n,f) cross section on the target spin in the energy region $E_n<1.5$ MeV. This effect is most prominent for target spins that involve strong populations of 1^+ and 0^- states in the compound nucleus. The fission of the $1/2^+$ isomer at 77 eV

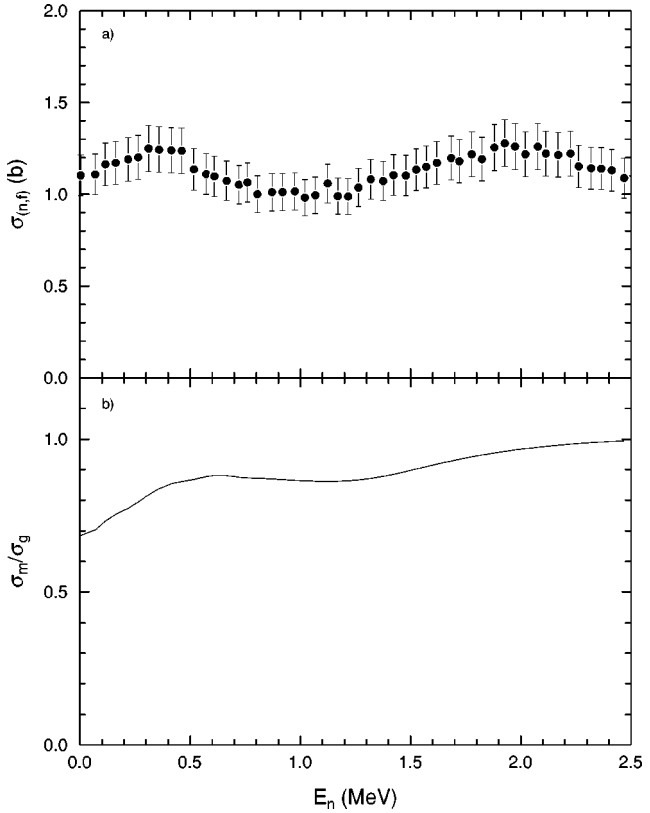

FIG. 11. Best-fit estimates of (a) the $^{235}U^m(n,f)$ cross section, and (b) the isomer-to-ground-state (n,f) cross section ratio. The error bars on $\sigma_{(n,f)}$ reflect a 10% systematic uncertainty in the $P_{(t,pf)}$ data.

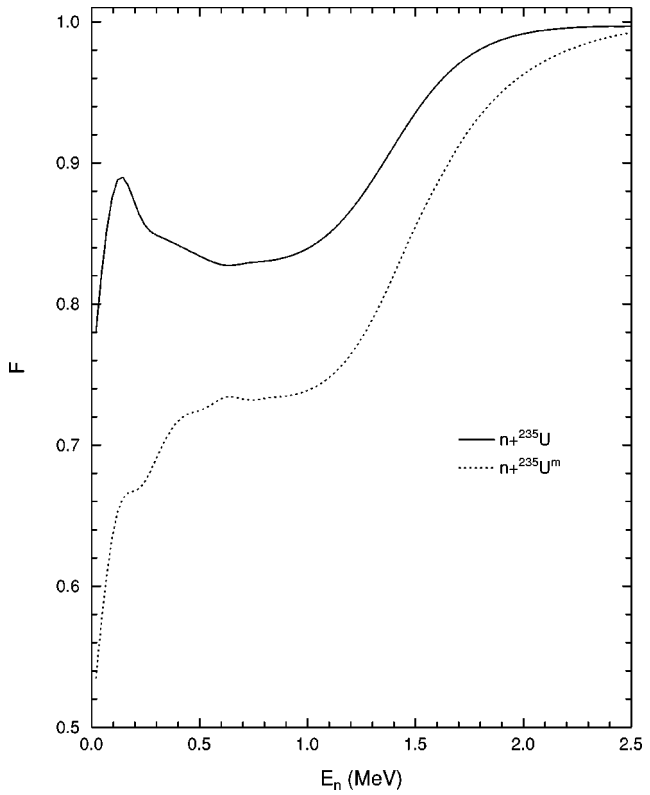

FIG. 12. Plot of the factor F defined in Eq. (7) for neutron-induced fission on both the ^{235}U ground state and isomer.

in ^{235}U will be inhibited at low neutron energies according to this model. Figure 11 shows predictions for $\sigma_{(n,f)}$ from this model and the ratio of predicted cross sections for the isomer and the ground state. The results show a decrease in $\sigma_{(n,f)}$ for the isomer of about 30% at 0.1 MeV which disappears slowly as the neutron energy increases to 2 MeV. This estimate relies on the premise that the only low-lying 1^+ states at the fission saddle points come from two-phonon excitation of the $K=0^-\otimes K=1^-$ and $K=1^-\otimes K=2^-$ bands and that the two phonon bands lie at approximately the sum energy for the individual vibrational excitations. Changes in the assumed position for the first 1^+ and 0^- would have quantitative but not qualitative effects on the results (see the Appendix). This relative inhibition of fission below 2 MeV could also be present in ^{237}U, ^{239}Pu, and ^{241}Cm all of which have a $1/2^+[743]$ ground state. Estimated (n,f) cross sections for ^{237}U will be presented in a subsequent paper. The present results for the $^{235}U^m$ isomer are in general agreement with similar calculations by Lynn and Hayes [25].

The effect of including spin and parity in the $P_{(t,pf)}$ calculations is quantified by the factor $F(E_n)$ defined in Eq. (7). This factor is plotted in Fig. 12 which shows that, for $E_n=0.1-2.5$ MeV, the effect of including J^π is at most $\sim$15% for neutron-induced fission of the ^{235}U ground state but, for fission induced on the isomer, the effect can be as large as $\sim$35%.

IV. DISCUSSION

We have shown that by modeling the angular-momentum dependence of the fission probability for ^{236}U it is possible to use measured $^{234}U(t,pf)$ data to simulate the $^{235}U(n,f)$ cross section to within nearly the accuracy of the (t,pf) data ($\pm$ 10%) over the incident neutron energy region from 0.1 to 2.5 MeV. With the model developed in this work it is also possible to predict the $^{235}U^m(n,f)$ cross section and the results show a significant decrease in $\sigma_{(n,f)}$ for the isomer relative to the ground state at energies below 2 MeV. This decrease can be understood in terms of a reduced probability for fission from 1^+ and 0^- states near the fission threshold. However, in order to obtain these quantitative results it was necessary to renormalize the calculated (t,pf) probability values obtained from the model to the experimental data. The renormalization procedure was necessary to smooth structure that appears in the model predictions due to uncertainties in the level densities in the matching regions between the discrete- and continuous-level regions.

In these results we see that to obtain quantitative estimates of $\sigma_{(n,f)}$ it is necessary to account for the differences in the angular-momentum distributions in the (t,pf) and (n,f) reactions. However, the angular-momentum effects are only important in the region $E_n<1$ MeV. At higher energies we find (Fig. 10) that the $P_f(E_x,J^\pi)$ distributions become independent of J^π because of a preponderance of decays to the continuous level-density region above the pairing gaps. In the continuous level-density region the levels in the first well and on top of the barriers have very similar spin distri-

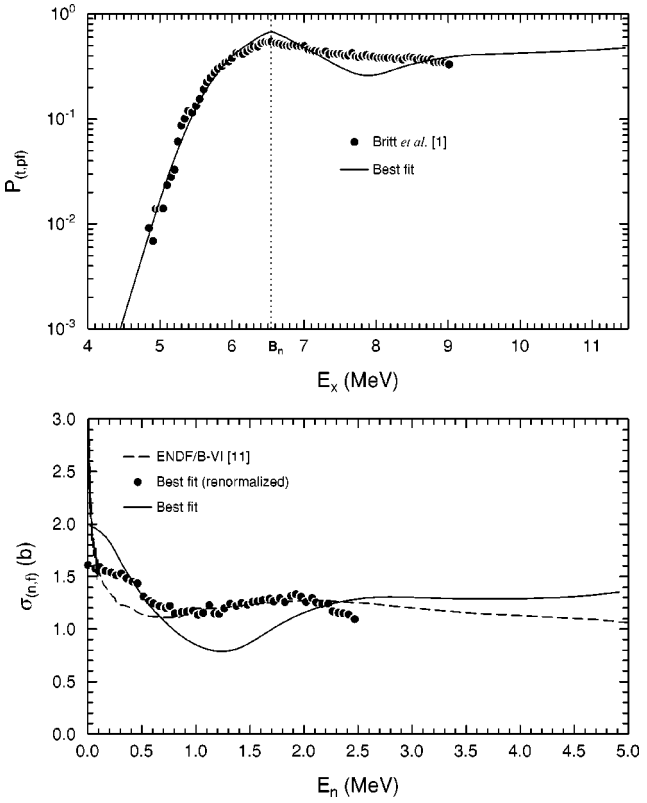

FIG. 13. Best fit extended to $E_x = 11.5$ MeV in ^{236}U (top panel). The vertical dotted line denotes the neutron-binding energy value. The bottom panel shows the (n,f) cross-section calculations extended up to $E_n = 5$ MeV (solid line). The filled circles represent the same renormalized calculation as in Fig. 9. The ENDF/B-VI evaluation is shown as a dashed line for comparison.

butions so that any spin dependence for the ratio N_f/N_n disappears. This result confirms the empirical observation in previous work [7,8].

A lower limit for the application of this technique is estimated to be approximately $E_n \sim 0.1$ MeV. This limit is consistent with the energy resolution in the (t,pf) measurement (120-keV full width at half maximum) and increasing uncertainties in the neutron transmission coefficients below 100 keV. Improved experiments and theory could in principle decrease both of these limits. However, extensions of the surrogate technique to $E_n < 100$ keV would apply only to energy-integrated cross sections. Thus for example, the measured isomer-to-ground-state ratio values of 1.61 ± 0.44 and 2.47 ± 0.45 [26] at cold- and thermal-neutron energies, respectively, could not be directly compared to the predictions of the technique because the ^{235}U(n,f) and ^{235}U$^m(n,f)$ cross sections are determined primarily by the properties of nearby resonances at these low energies.

It would be valuable to have a fission model that, when fit to data in the barrier region, could predict $P_{(t,pf)}$ and $\sigma(n,f)$ values up to equivalent neutron energies of 5 MeV or more. The renormalization technique used in this paper limits the applicability of our model to the range of available experimental data. However, if the need to renormalize is due primarily to problems in the level density regions where discrete bands are matched to the continuous densities, then extrapolations to higher energies could be attempted albeit with increased systematic uncertainties. To test this idea the calculations for $n + ^{235}$U were extended to $E_n = 5$ MeV and the results are shown in Fig. 13. The predicted $\sigma(n,f)$ points in Fig. 13 increase slowly and smoothly above 2 MeV and are approximately 30% greater than the ENDF/B-VI value at $E_n = 5$ MeV. It is possible that small changes in the barrier parameters could give an even better fit. This result suggests that the undershoot in the excitation energy region of 8 MeV may be due to local mismatching of the level densities at the pairing gaps as speculated above. This question and the general refining of the model to allow extrapolation to higher energies will be addressed in a subsequent paper that will contain the results of systematic fits to the series of Th, U and Pu isotopes available from past (t,pf) measurements and some of the odd-Z nuclei that have been studied using ^{3}He-induced direct fission measurements.

TABLE I. Description of sensitivity-analysis tests.

Test No.	Description
1	Replaced discrete levels with continuum level density in ^{235}U.
2	Eliminated all two-phonon transition states above the barriers.
3	Used transmission coefficients from the ABACUS calculation.
4	Assumed twice as many positive- as negative-parity states in 1^{st} wells of ^{236}U and ^{235}U, affecting γ and neutron decays as well as the formation processes.
5	Used constant $P_{(t,p)}(J^\pi)$ population probability up to $J = 10$, zero for $J > 10$.
6	Fit entire E_x energy range of $P_{(t,pf)}$ data, varying all three barrier heights.
7	Scaled 1^{st}-well continuum level density by 2.5 in ^{236}U and by 2.0 in ^{235}U to match known level spacings at the neutron binding energy.
8	Used double-Lorentzian dependence for γ-ray strength function instead of E_γ^3 form in Eq. (10).
9	Raised all two-phonon energies by 30% for transition states above the barriers.
10	Scaled the discrete-level contribution to N_n by the factor 0.58 to eliminate the dip in the calculated $P_{(t,pf)}(E_x)$ curve.
11	Set $\hbar\omega_A = 0.65$.
12	Set $\hbar\omega_B = 0.90$.
13	Turned off width-fluctuation correction for both fission and neutron emission.
14	Fit without B_{II} barrier.

ACKNOWLEDGMENTS

We are grateful to Frank Dietrich for providing new calculations of neutron transmission coefficients and for many useful discussions on the development of the model. Valuable input on this project came from continuing discussions with John Anderson, John Becker, Daniel Gogny, Dennis McNabb, André Michaudon, Erich Ormand, and Morton Weiss. This work was performed under the auspices of the

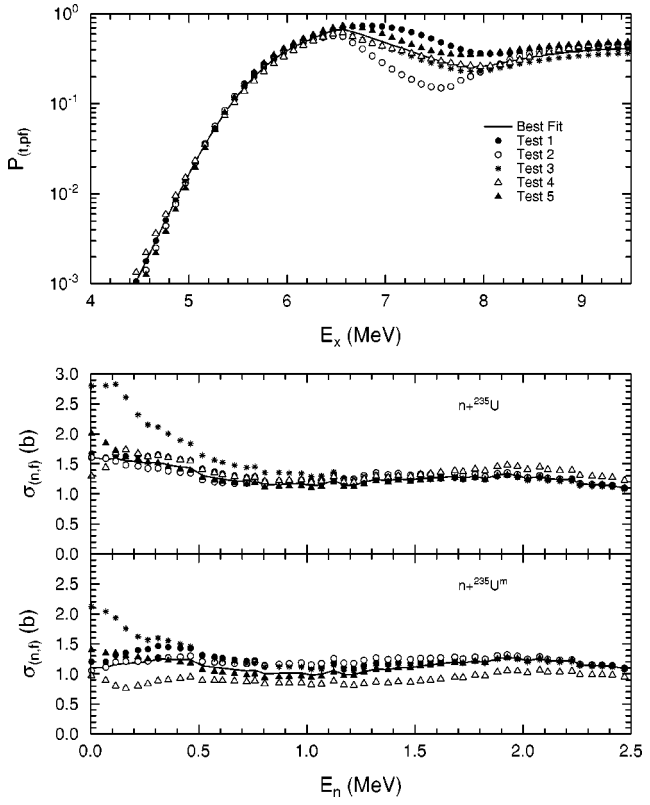

FIG. 14. Sample of sensitivity tests for the estimated (n,f) cross section on the ^{235}U ground state and isomer. A description of the various tests can be found in Table I.

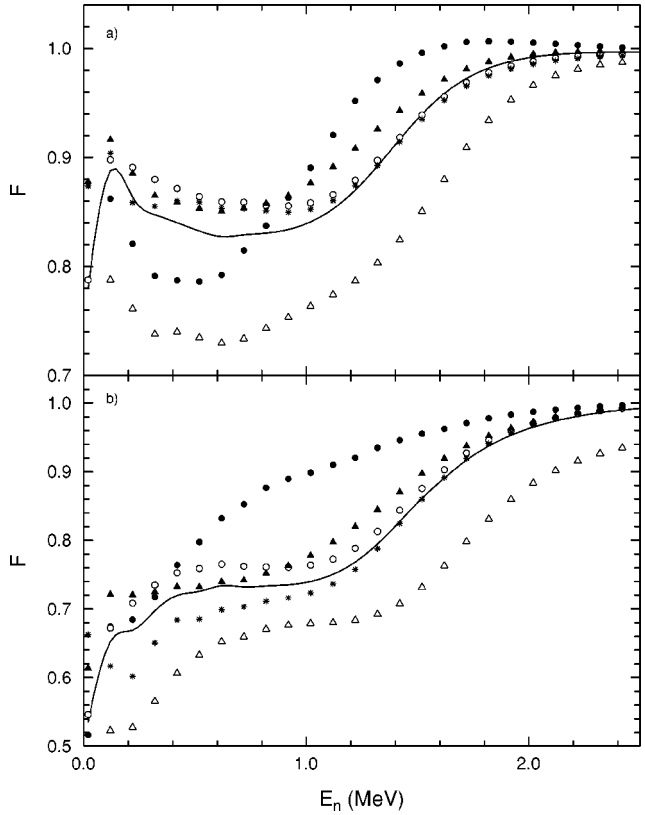

FIG. 15. Sensitivity of the factor F defined in Eq. (7) to the tests described in Table I for the (a) $n+^{235}$U, and (b) $n+^{235}U^m$ reactions. The legend is the same as in Fig. 14.

U.S. Department of Energy by the University of California, Lawrence Livermore National Laboratory under Contract No. W-7405-Eng-48.

APPENDIX: SENSITIVITY ANALYSIS

In this appendix the $\sigma_{(n,f)}$ calculations described in the main body of the paper are subjected to a series of sensitivity tests. These tests will show that the final cross section results are insensitive to all but a few factors in the model. The robustness of the results is due in large part to the renormalization of the $\sigma_{(n,f)}$ calculations to the $P_{(t,pf)}$ data. This renormalization procedure, described by Eq. (6) partitions the calculated (n,f) cross section into three contributions: the measured fission probabilities $P_{(t,pf)}$, the calculated neutron-capture cross section σ_{CN}, and the factor F defined in Eq. (7). The first factor, $P^{(\mathrm{expt})}_{(t,pf)}$ is purely experimental, σ_{CN} is largely determined by the neutron transmission coefficients, and the factor F is influenced primarily by the number of open discrete fission and neutron channels for $E_n \lesssim 1$ MeV and becomes model independent at higher energies.

A set of sensitivity tests is detailed in Table I, and a selection of these is shown in Fig. 14. The $F(E_n)$ curves corresponding to the tests plotted in Fig. 14 can be found in Fig. 15.

In test 1 the continuum level density in ^{235}U was extended down to the ground state, replacing the discrete levels. This variation mitigates the ''dip'' in the calculated $P_{(t,pf)}$ probabilities by effectively reducing the number of low-lying levels in ^{235}U compared to the best-fit result. The effect on calculated cross sections is most readily seen in the case of neutron-induced fission on the ^{235}U isomer where the calculated $\sigma_{(n,f)}$ values in this test overshoot the best-fit curve. In practice, the discrete levels in ^{235}U are well known up to the pairing gap, and it is not necessary to lower the matching point between discrete and continuum regions. In the same spirit, the contribution to N_n from discrete states was scaled back in test 10 to reduce the dip in calculated $P_{(t,pf)}$ values, with less than a 6% change in the cross sections on either ground or isomeric states in ^{235}U.

Removing all two-phonon states above the barriers, as was done in test 2, mostly affects the fit to the $P_{(t,pf)}$ data and the $n+^{235}U^m$ cross-section calculation. In this test, it was necessary to supplement the reduced number of discrete states above the barriers by replacing the discrete spectrum with a constant level density function from about 900 keV in excitation energy up to the pairing gaps. This prescription actually introduces a higher density of 0^- and 1^+ states than is shown for the best-fit calculation in Fig. 3. As a consequence, the calculations performed under test 2 produced an isomer-to-ground-state cross-section ratio slightly higher than the one shown in Fig. 11, rising to 1 at $E_n \approx 0.6$ MeV. A less drastic modification of the discrete levels above the fission barriers was carried out in test 9, where the two-phonon state energies were raised by 30% to mimic the effect of anharmonicities in the vibration. In that case, the resulting

$\sigma_{(n,f)}$ cross sections deviate by less than 6% from the best-fit values.

The most striking departure from the best fit occurs for test 3 where an older set of transmission coefficients, produced using the code ABACUS [7], was used. Interestingly, there is essentially no difference between the $F(E_n)$ values calculated with either the older or current transmission coefficients (see Fig. 15). Therefore the transmission coefficients primarily affect the capture cross-section calculation.

In test 4 the density of positive-parity states was increased to twice the density of negative-parity states in the first wells of ^{235}U and ^{236}U. This change was motivated by the dearth of negative-parity orbitals near the Fermi surface for the actinides and it affects the calculated fission probabilities $P_f(E_x, J^\pi)$ as well as the formation probabilities $P_{(t,p)}(J^\pi)$ and $P_{CN}(E_x, J^\pi)$. These changes produce a noticeable variation in the calculated $F(E_n)$ values (Fig. 15). The resulting effect can most clearly be seen in the neutron-induced cross section on the $^{235}U^m$ isomer. However, the factor-of-two enhancement of positive-parity states is very likely excessive, and the difference in density between the two parities should quickly disappear with excitation energy.

The effect of a significant change to the (t,p) formation probability was investigated in test 5. The changes in the calculated $\sigma_{(n,f)}$ values are confined to the region below $E_n \approx 200$ keV. More realistic variations of $P_{(t,p)}$ obtained by altering the input parameters in the DWBA calculations within reasonable limits produce negligible changes in the resulting (n,f) cross sections.

Additional tests are described in Table I, but not shown in Figs. 14 and 15. These tests did not produce significant changes in the calculated $\sigma_{(n,f)}$ values (i.e., less than $\pm 15\%$ deviations from the best fit for fission on either the ground state or the isomer in ^{235}U for $E_n \geqslant 100$ keV).

[1] H. C. Britt, F. A. Rickey, and W. S. Hall, Phys. Rev. **175**, 1525 (1968).

[2] J. D. Cramer and H. C. Britt, Phys. Rev. C **2**, 2350 (1970).

[3] B. B. Back, Ole Hansen, H. C. Britt, and J. D. Garrett, Phys. Rev. C **9**, 1924 (1974).

[4] B. B. Back, H. C. Britt, Ole Hansen, B. Leroux, and J. D. Garrett, Phys. Rev. C **10**, 1948 (1974).

[5] A. Gavron, H. C. Britt, E. Konecny, J. Weber, and J. B. Wilhelmy, Phys. Rev. C **13**, 2374 (1976).

[6] A. Gavron, H. C. Britt, P. D. Goldstone, R. Schoenmackers, J. Weber, and J. B. Wilhelmy, Phys. Rev. C **15**, 2238 (1977).

[7] J. D. Cramer and H. C. Britt, Nucl. Sci. Eng. **41**, 177 (1970).

[8] H. C. Britt and J. B. Wilhelmy, Nucl. Sci. Eng. **72**, 222 (1979).

[9] L. A. Bernstein, *et al.*, Phys. Rev. C **65**, 021601 (2002).

[10] *Scientific opportunities with an advanced ISOL facility*, http://www.er.doe.gov/production/henp/isolpaper.pdf (1997).

[11] L. W. Weston, P. G. Young, W. P. Poenitz, and C. R. Lubitz, ENDF/B-VI evaluation, MAT # 9228, Revision 5, October 1997; data retrieved from the ENDF database.

[12] A. Gavron, H. C. Britt, P. D. Goldstone, J. B. Wilhelmy, and S. E. Larsson, Phys. Rev. Lett. **38**, 1457 (1977).

[13] C. E. Porter and R. G. Thomas, Phys. Rev. **104**, 483 (1956).

[14] B. B. Back, J. P. Bondorf, G. A. Ostroschenko, J. Pedersen, and B. Rasmussen, Nucl. Phys. **A165**, 449 (1971).

[15] P. A. Moldauer, Phys. Rev. **123**, 968 (1961).

[16] S. F. Mughabghab and C. L. Dunford, in *Proceedings of the International Conference on the Physics of Nuclear Science and Technology* (American Nuclear Society, New York, 1998), Vol. 1, p. 784.

[17] M. R. Schmorak, Nucl. Data Sheets **69**, 375 (1993), data extracted from the ENSDF database, revision of June 1, 1993.

[18] M. R. Schmorak, Nucl. Data Sheets **63**, 183 (1991); data extracted from the ENSDF database, revision of March 1, 1991.

[19] H. C. Britt, in *Proceedings of the Fourth International Symposium on the Physics and Chemistry of Fission*, Julich, West Germany (International Atomic Energy Agency, Vienna, 1979), Vol. 1, p. 3.

[20] J. J. Griffin, in *Proceedings of the Symposium on Physics and Chemistry of Fission*, Salzburg, 1965 (International Atomic Energy Agency, Vienna, 1965), Vol. 1, p. 23.

[21] S. Bjørnholm, A. Bohr, and B. R. Mottelson, in *Proceedings of the Third International Symposium on the Physics and Chemistry of Fission*, Rochester, 1973 (International Atomic Energy Agency, Vienna, 1974), Vol. 1, p. 367.

[22] P. D. Kunz, *The dwuck4 code*, http://spot.colorado.edu/ kunz/DWBA.html

[23] F. S. Dietrich (private communication).

[24] P. G. Young, E. D. Arthur, and M. B. Chadwick, *Comprehensive Nuclear Model Calculations: Introduction to the Theory and Use of the GNASH Code*, Tech. Rep. LA-12343-MS, Los Alamos National Laboratory (1992).

[25] J. E. Lynn and A. C. Hayes, Phys. Rev. C **67**, 014607 (2003).

[26] A. D'Eer, C. Wagemans, M. Nève de Mévergnies, F. Gönnenwein, P. Geltenbort, M. S. Moore, and J. Pauwels, Phys. Rev. C **38**, 1270 (1988).